FAST. ACCURATE. TRUSTED.

RIT™

Everything you would expect from Medical Physics' leading QA software for over 25 years, plus **so much more**.

LET RIT'S NEW SOFTWARE UPGRADE EXCEED YOUR EXPECTATIONS:

THE RIT FAMILY OF PRODUCTS **VERSION 6.7.X**

- Achieve sub-pixel accuracy with the enhanced 3D Winston-Lutz (Isocenter Optimization) routine.
- Perform efficient and accurate Elekta Leaf Speed Analysis, with minimal setup.
- Cerberus 2.0: Completely streamline your imaging QA workflow with hands-free automation.
- Set custom tolerance values for every measurement used in automated phantom analyses with RIT's new Tolerance Manager.
- Easily perform exact dose comparisons with TomoTherapy® Registration for Patient QA.
- Manage software licenses at your convenience with RIT's new, cloud-based system.
- Fully-customize your software experience with RIT's updated, dynamic interface.

DEMO VERSION 6.7.X AT ASTRO 2018: BOOTH #2025

RADIOLOGICAL IMAGING TECHNOLOGY, INC.

RADIMAGE.COM

(+1) 719.590.1077 x211 // sales@radimage.com

Connect with RIT @RIT4QA

A dynamic ultrasound simulation of a pulsating three-layered CCA for validation of two-dimensional wall motion and blood velocity estimation algorithms

Xiao Hu, Yufeng Zhang,[a)] and Guanghui Cai
Department of Electronic Engineering, Information School, Yunnan University, Kunming, Yunnan 650091, China

Kexin Zhang
Department of Cardiovascular, The Second Affiliated Hospital of Kunming Medical University, Kunming, Yunnan 650031, China

Li Deng, Lian Gao, Suya Han, and Jianhua Chen
Department of Electronic Engineering, Information School, Yunnan University, Kunming, Yunnan 650091, China

(Received 24 April 2017; revised 13 October 2017; accepted for publication 23 October 2017; published 10 December 2017)

Purpose: A dynamic ultrasound simulation model for the common carotid artery (CCA) with three arterial layers for validation of two-dimensional wall motion and blood velocity estimation algorithms is proposed in the present study. This model describes layers with not only characteristics of echo distributions conforming to clinical ones but also varying thicknesses, axial, and radial displacements with pulsatile blood pressure during a cardiac cycle.
Methods: The modeling process is as follows: first, a geometrical model according with the clinical structure size of a CCA is built based on the preset layer thicknesses and the diameter of lumen. Second, a three-dimensional scatterer model is constructed by a mapping with a Hilbert space-filling curve from the one-dimensional scatterer distribution with the position and amplitude following Gamma and Gaussian distributions, respectively. The characteristics of three layers and blood are depicted by smoothly adjusting the scatterer density, the scale, and shape parameters of the Gamma distribution as well as the mean and standard deviation of the Gaussian distribution. To obtain the values of parameters of scatterer distributions, including the shape parameter, density, and intensity, for arterial layers and blood, the envelope signals simulated from different configurations of scatterer distribution are compared with those from different kinds of tissue of CCAs *in vivo* through a statistic analysis. Finally, the dynamic scatterer model is realized based on the blood pressure, elasticity modulus of intima-media (IM) and adventitia, varying IM thickness, axial displacement of IM as well as blood flow velocity at central axis during a cardiac cycle. Then, the corresponding radiofrequency (RF) signals, envelope signals, and B-mode images of the pulsatile CCA are generated in a dynamic scanning mode using Field II platform.
Results: The three arterial layers, blood, and surrounding tissue in simulated B-mode ultrasound images are clearly legible. The results based on a statistical analysis for the envelope signals from 30 simulations indicate that the echo characteristics of blood, intima, media, and adventitia are in accordant with clinical ones. The maximum relative errors between the preset geometrical sizes and the measured ones from the simulated images for the diameter of the lumen and the thicknesses of the intima, media, and adventitia are 0.13%, 3.89%, 1.35%, and 0.06%, respectively. For the dynamic parameters, the variation in IM thickness, the radial displacements of lumen and adventitia as well as the axial displacement of IM and blood flow velocity are measured with the mean relative errors of 68.03%, 9.27%, 2.10%, 4.93%, and 17.34%, respectively.
Conclusion: The simulated results present static sizes and dynamical variations according with preset values; echo distributions conforming to clinical versions. Therefore, the presented simulation model could be useful as a data source to evaluate the performance of studies on measurements of ultrasound-based tissue structures and dynamic parameters for the CCA layers. [https://doi.org/10.1002/mp.12678]

Key words: common carotid artery, pulsation in axial and radial directions, three-layered arterial wall, ultrasonic model

1. INTRODUCTION

Owing to high rates of morbidity and mortality, it has increasingly become a research emphasis on detection of pathological changes occurring in intravascular histology and morphology to identify the severity of cardiovascular diseases.[1,2] Researches have shown that the first sign of cardiovascular disease is intima-media (IM) thickening of arterial walls.[3] However, the latest pathophysiological studies also suggest that the tissue structures of the intima, media, and adventitia of a common carotid artery (CCA), and their dynamic features in axial and radial directions during a cardiac cycle could be used to

more early and accurately characterize the symptoms of cardiovascular diseases. As a progressive, chronic, and asymptomatic vascular disease, atherosclerosis originates from the subendothelial accumulations of foam cells causing small lesions. Then, the plaques are present and become complex with calcification to evolve to advanced lesions from the media of the vessel wall. Thereafter, the lesions grow toward the adventitia, and finally expand to outward and encroach on the lumen.[4] Rodriguez–Macias[5] individually observed the thicknesses of the intima and media as well as the ratio of intima to media in the CCAs of 100 consecutive 70-year-old human subjects. They found the thicker intima layer and thinner media layer for those subjects with cardiovascular disease, myocardial infarction, or stroke compared with healthy subjects. In Falk et al.'s study,[6] the arterial adventitia made response to various kinds of arterial injuries by clinical manifestation and data analysis from four pathological entities containing the adventitial lymphoid neogenesis in chronic rejection, the adventitial inflammation and fibrosis in abdominal aortic aneurysm as well as the adventitial angiogenesis in atherosclerosis. This indicates that the vessel wall response to injury principally occurs in the adventitia and directly or indirectly affects the biology of the entire vessel wall and surrounding tissue. Thus, the measurements for tissue structures, thickness changes as well as axial and radial pulsations of each layer of CCAs could be important for early detection, treatment, and prevention of cardiovascular diseases.

With real-time, noninvasive, and low-cost advantages, ultrasonic technique is commonly used not only to image the vascular tissue structure and its kinestate but also to measure and locate vessels. It is also the preferred method for detecting the three layers of arterial walls.[7–11] Ahlgren et al.[7] first proposed simultaneous measurements of the axial and radial displacements of an arterial wall *in vivo* using a noninvasive ultrasonic method. In this method, a region-of-interest (ROI) with fixed size was designated, and a kernel with smaller size was selected automatically in the middle of the ROI. Then, the axial and radial displacements of an arterial wall were measured by estimating cross-correlation coefficients between the ROI and kernel in the successive frames. On this basis, an ultrasonic echo-tracking method based on two cross-correlations was presented to measure the arterial wall movements *in vivo*.[8] To obtain the maximum cross-correlation coefficient for an optimal fitting position, two cross-correlations (one is between the kernel and ROI in the first frame; another is between the kernel in the first frame and the ROI in the succeeding frame) were calculated, and the axial and radial displacements of arterial wall were found. Subsequently, two comparative studies were made using the above-mentioned method to find the motion mode of axial displacements of IM in the CCA during a cardiac cycle, respectively. The first one was implemented for the consecutive measurements on the CCA in 20 healthy human subjects;[9] the second one was for the measurements of the right CCA in ten healthy humans 4 months apart.[10] However, these researches are preliminary studies based on clinical data. The errors in the indices obtained directly from human subjects are unknown, and the accuracy and reliability of experimental results are hard to be validated. Additionally, it is also difficult to accurately measure the dynamic parameters such as the thickness variations and the modes of motion for layers in a CCA using the ultrasound, because the thicknesses and their variations of three layers, especially for the intima and media, are less than a millimeter. Moreover, the differences in the tissue structure of layers cause different distributions in the ultrasonic echoes and then different speckle patterns on B-mode images.[5–11]

Computerized ultrasound simulation models with high controllability and verisimilitude are commonly used as data sources for the performance evaluation of studies related to the measurements of tissue structures, thickness variations as well as axial and radial displacements of the intima, media, and adventitia in the CCA.[12] In simulation models, different types of ground truth could be preset, and then, the estimated results could be compared with the preset values for evaluating estimation algorithms. For these reasons, several researchers made a series of studies about the ultrasonic simulation methods for CCA. Balocco et al.[13] introduced a three-dimensional (3D) ultrasound model for the CCA with a single layer using generalized cylinders to express the IM and surrounding tissues. This phantom was regulated by defining a uniform distribution for the scatterer position and a Gaussian distribution for the scatterer amplitude. Then, the radiofrequency (RF) signals, envelope signals, M-mode images, and B-mode images were generated in Field II. This ultrasound model could be used as a tool of the preliminary evaluation for the threshold segmentation based on the M-mode images and the estimation of blood flow velocity. Warriner et al.[14] presented a simulating Doppler ultrasound model for the pulsatile blood flow and single layer within elastic and viscoelastic arteries. In this model, the blood flow dynamic was simulated by the nonlinear Navier–Stokes equations; the wall viscoelasticity and tethering extension were established using the Voigt model and equations of motion by Womersley, respectively. Matlab was used to gain the pulse Doppler ultrasound signals. A kinematic cylindrical model of the carotid artery with single layer was constructed in silico by Larsson et al.[15] The scatterers of this model with the density of the Rayleigh limit were randomly positioned and moved radially based on the time-dependent distention of IM measured *in vivo* in a healthy young. The B-mode images were simulated using a generalized convolution algorithm, and the normalized cross-correlation was calculated on both the RF signals and the envelope-detected signals to extract longitudinal and radial motion for testing validity. A method for simulating the ultrasound videos of a CCA with three arterial layers was proposed by Solomou et al.[16] The grayscales of intima, media, and adventitia of CCA images were set as the median levels estimated from clinically scanned B-mode images. The motions of the walls in radial and axial directions were followed using the specialized motion analysis and segmentation software toolbox developed by their own group. The random noise was added to images to form the artificial speckle. However, the motion curve and speckle distribution were significantly different from the clinical ones. Fekkes et al.[17] simulated

ultrasound images for a 3D atherosclerotic carotid artery with two layers at the bifurcation using Field II based on the plane-wave imaging technique. The lumen shape was created by an approximate lumen segmented from a patient. The deformation states in radial and circumferential directions were calculated using a patient-specific finite element model based on ABAQUS software. Stoitsis et al.[18] simulated dynamic B-mode ultrasound images for the CCA with three layers. However, the scatterer distributions for all three layers were set to be the same. A real B-mode ultrasound image was used as a template to map the scatterers' amplitude. The motion of arterial walls in radial and axial directions was approximately described by an exponential function and a simple sinusoidal function. Thus, the existing ultrasound simulation models of the CCA suffer from limitations to some extent, such as the single layer structure, identical scatterer distribution for different layers, unvarying IM thickness, or unrealistic speckle distribution and wall motion during a cardiac cycle.

For this purpose, a dynamic ultrasound simulation model for the CCA with three layers for validation of two-dimensional (2D) wall motion and blood velocity estimation algorithms is proposed in the present study. The model describes arterial layers with not only characteristics of echo distributions conforming to clinical ones but also varying thicknesses and axial and radial displacements with pulsatile blood pressure during a cardiac cycle. The modeling process is as follows: first, a geometrical model according with clinical structure size of a CCA is built based on the preset thicknesses of layers and the diameter of lumen. Second, a 3D scatterer model is constructed by a mapping with a Hilbert space-filling curve from the one-dimensional (1D) scatterer distribution with the position and amplitude following Gamma and Gaussian distributions, respectively. The characteristics of three layers and blood are depicted by smoothly adjusting the scatterer density, the scale and shape parameters of the Gamma distribution as well as the mean and standard deviation (SD) of the Gaussian distribution. To obtain the values of parameters of scatterer distributions, including the shape parameter, density, and intensity, for arterial layers and blood, the envelope signals simulated from different configurations of scatterer distribution are compared with those from different kinds of tissue of CCAs *in vivo* through a statistic analysis. Finally, the dynamic scatterer model is realized based on the blood pressure, elasticity modulus of IM and adventitia, varying IM thickness, axial displacement of IM as well as blood flow velocity at central axis during a cardiac cycle. Then, the corresponding radiofrequency (RF) signals, envelope signals, and B-mode images of the pulsatile CCA are generated in a dynamic scanning mode using Field II.

2. MODEL BUILDING

2.A. Ultrasound simulation based on field II program

Field II[19] is an ultrasound simulation program under the Matlab using the concept of spatial impulse response and linear system theory based on the acoustical principle. This allows simulating different ultrasound probes, acoustic fields produced by tissue, ultrasound images, etc. The geometry, density, amplitude, and tissue structure of a scatterer model as well as the parameters about probes and scanning functions can be flexibly adjusted to generate ultrasound images. With a variable scatterer density, position distribution, amplitude distribution, and geometrical structure, the scatterer model can correspondingly generate the echoes with speckle distributions ranging from tightly clustered to random to nearly regular to mimic a broad range of tissue types. The different kinds of ultrasound transducer and related images can be simulated, and the transducer focusing and apodization can also be dynamically controlled in Field II.

2.B. CCA geometric model with three layers

The geometric model of CCA with three layers is constructed with generalized cylinders, whose diameters and lengths are set according to an anatomic dimension.[20] Four concentric generalized cylinders with the diameters of 5.25 mm, 5.55 mm, 6.55 mm, and 7.35 mm, and the length of 20.00 mm is used to model the artery with the lumen diameter of 5.25 mm and the thicknesses of intima, media, and adventitia of 0.15 mm, 0.5 mm, and 0.4 mm, respectively. The geometric model is shown in Fig. 1.

2.C. Scatterer model for CCA with three layers and blood

2.C.1. Scatterer model

The organization structure is generally depicted by the model for a scatterer distribution when an ultrasound simulation for the biological tissue is carried out. It is assumed that the tissue takes the form of many discrete scatterers distributed in 3D space. The characteristics of different tissue structures are described by the clustered, random, and regular patterns in position distribution as well as the distribution of the ultrasonic reflection intensity. In a CCA, the tissue properties and structures for the intima, media, and adventitia and blood are different. Thus, when the scatterer model for a CCA is established, the varying patterns in the scatterer distribution adjusted by the parameters of clustering,

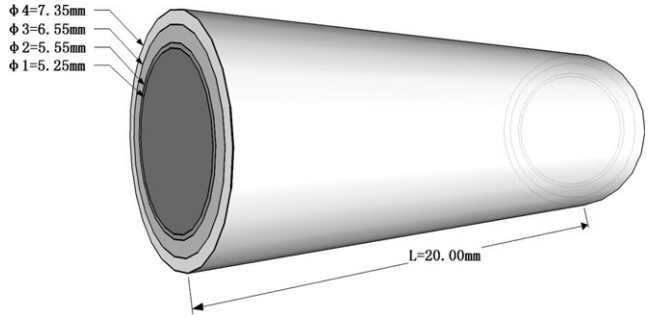

FIG. 1. The schematic diagram for the 3D geometrical construction of the CCA with three layers.

randomness, density, and intensity should be considered. At present, several scatterer models including the Neyman–Scott model,[21] Gibbs–Markov model,[22] and Cramblitt model[23] have been proposed. Among them, the Cramblitt model is demonstrated as a flexible and realistic method to produce a scatterer distribution with varying density and spatial organization ranged from tightly clustered to random to nearly regular for mimicking a broad range of tissue types.

In the 1D marked regularity model developed by Cramblitt, scatterers are considered as the points of a stationary renewal point process a specific Poisson point process. Then, the original 1D random scatterer function is expressed as:

$$s(x) = \sum\nolimits_i g_i \delta(x - X_i) \tag{1}$$

where g_i and X_i denote the strength and the ordered sequence for the position of scatterers, respectively. In this model, scatterers are randomly distributed with the distance $d_i = |X_i - X_{i-1}|$ following Gamma distribution with shape parameter α and scale parameter β:

$$f(d) = \frac{d^{\alpha-1} e^{-x/\beta}}{\Gamma(\alpha)\beta^{\alpha}}, \quad \alpha, \beta, d > 0 \tag{2}$$

where $\Gamma(\alpha)$ is Gamma function. The mean and variance of this distribution are $\bar{d} = \alpha\beta$ and $\sigma_d^2 = \alpha\beta^2 = \bar{d}^2/\alpha$, respectively. Therefore, the scatterer distribution could be tuned by the shape parameter α if the mean distance $\bar{d}$ is given. For $\alpha < 1$, the scatterer distribution has a higher variance, and the scatterers present clustered tendency. With $\alpha = 1$, the scatterer distribution turns to an exponential distribution, and the scatterers are randomly distributed. If $\alpha > 1$, the point spacing has a lower variance, and scatterers are placed regularly. The distance between the adjacent scatterers is equivalent in extreme cases. By presetting different α, the scatterer distribution could be regulated along a continuum from clustered to random, even to regular. This yields a flexible and continuously adjustable scatterer model.

To ensure the scatterer isotropy in the space, the 1D scatterer should be mapped to the 3D space. This is realized by a mapping with a 3D Hilbert space-filling curve[24] from the 1D scatterer distribution. As a mapping from 1D to *N*-D space, the Hilbert space-filling curve is a continuous and nondifferentiable fractal curve. It keeps the correlation of the adjacent scatterers in the original space. Figure 2 shows the mapping from 1D to 3D space. Scatterers in 1D space start from a vertex of a cube cell to another along a side of this cube until all cube cells are traversed in the 3D space in sequence, where the vertical number of the cube indicates the filling path.

2.C.2. Statistic model for echo envelope signals

Analysis of the envelope signals echoed from tissue using a statistic model, such as Rayleigh, K, Rician, and Nakagami distributions, is a common means to quantitatively describe the tissue organization and characterization. Previous researches[25] suggested that the Rayleigh model is suitable for describing the echoes from the tissue with a large number of scatterers per resolution cell without a deterministic component; the K distribution works well with sparse scatterers and nonexistence of a deterministic component; the Rician model is suited to a high density of scatterers with a deterministic component. For the envelope signals echoed from the tissue with a complex structure, the Nakagami distribution presents a great generalization ability and simple calculation.[26] Its probability density function is defined by

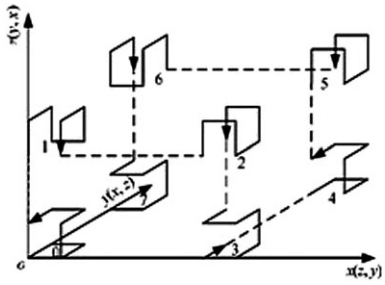

FIG. 2. The schematic diagram of the 3D Hilbert curves for scatterer mapping.

$$f(x) = \frac{2^{m^m}}{\Gamma(m)u^m} x^{2m-1} e^{-\frac{m}{u}x^2} \tag{3}$$

where m and u are shape and average power parameters, respectively, and $\Gamma(m)$ is the gamma function of order m. The flexibility of the Nakagami distribution can be understood by noting that this model is changed to post-Rayleigh or Rician distribution with $m > 1$, shades into pre-Rayleigh or generalized Rician distribution for $m < 1$, and corresponds to the Rayleigh model when $m = 1$.

2.C.3. Parameter identification for the scatterer model of CCA

To illustrate the relationship between the parameters of the scatterer model and the distribution of the simulated envelope signals, the scatterer model with different values of density and shape parameters are built firstly. Then, Field II is used to simulate echo envelope signals, from which the parameters of the Nakagami distribution are obtained by the maximum likelihood estimation (MLE).[27] Meanwhile, the echo envelope signals of blood in lumen, intima, media, and adventitia from clinical CCAs are also analyzed with Nakagami distribution by the MLE to generate their clinical parameters. Compared the parameters of the Nakagami distributions between the simulated and clinical echo envelope signals, the density and shape parameters of the scatterer model for the blood, intima, media, and adventitia of CCA are determined.

2.D. Pulsatile models of CCA with three layers and blood flow

Elastic carotid walls suffer radial deformation in the form of expansion and contraction with a pulsation variation in the blood pressure during a cardiac cycle *in vivo*. Simultaneously, by the effects of adventitial traction, tethering, and flowing blood, the longitudinal movement for IM is also non-

negligible.[28] For the motion in the radial direction, McDonald[29] proposed an isotropous pulse model with elasticity to describe the relationship between the radial displacement and blood pressure as:

$$d(t) = \frac{1.5R_i^2 R_o}{E(R_o^2 - R_i^2)}[P(t) - P_{\text{mean}}(t)] \quad (4)$$

where E represents the elastic modulus of the vessel wall; $P(t)$ and $P_{\text{mean}}(t)$ are the waveform and mean value of blood pressure; R_i and R_o are the internal and external radiuses, respectively. For the geometric model of CCA with three layers shown in Fig. 1, the internal and external radii of the vascular wall are the cylindrical radii of 2.625 mm and 3.675 mm, respectively. Meanwhile, under the action of blood pressure, the IM is compressed with a maximum value of 0.06 mm during a cardiac cycle.[10] Thus, an extra motion should be calculated with a measured variation curve of the IM thickness and added to the displacements of IM. The vascular stress is derived from blood pressure, longitudinal traction out of tethering, and adjacent vascular tissue.[30] Hence, IM has also a pulsatile displacement along the vascular axis direction under the longitudinal tensile stress. However, this axial motion is a varying pattern without a definite model. To get a realistic simulation, an axial displacement curve of IM extracted from a healthy subject is directly used to describe its pulsatile motion in the longitudinal direction.

For the blood velocity profile in healthy artery, Fung[31] presented a simple computation method. It assumes that the blood flow presents the tendency of laminar flow, and it means that the variation in the blood flow is unrelated to the vascular length and time. Consequently, the Poiseuille profile approximation is used to describe the velocities of blood flow in the different position of the lumen as follows:

$$v(r) = \left(1 - \frac{r^2}{R_L^2}\right)v_0 \quad (5)$$

where r represents the distance between the one point and the vascular center axis in the lumen; R_L and v_0 are the lumen radius and axial centerline velocity of blood flow, respectively. The pulsation curve for the axial centerline velocity of blood flow during a cardiac cycle can be measured using the ultrasonic technique.

The radial displacement of IM, radial displacement of adventitia, axial displacement of IM, and profile of blood flow during a cardiac cycle are applied to the established scatterer model of the intima, media, adventitia, and blood, respectively. The scatterer at a different position correspondingly moves in chronological order. Then, the pulsatile scatterer model of CCA with three layers and blood flow is constructed.

3. RESULTS AND DISCUSSION

3.A. Scatterer model

To explain the link between the parameters of the scatterer model and the distribution of the simulated echo envelope signals, the isotropous scatterer distributions based on different density and shape parameters are built. Figure 3 shows the scatterer distributions in a size of 8 × 8 mm from the Gamma model with different values of shape parameter α and density parameter ρ. The amplitudes of the scatterers follow a normal distribution with the mean of 0.5 and the variance of 0.2. In Fig. 3, the scatterer distributions can be found more clustered with a decrease in the value of α especially for $\alpha = 0.01$. As α increased, the gathered scatterers are gradually turning into random, or even uniform distributions, particularly for $\alpha = 100$. On the other hand, increased value of parameter ρ yields a denser distribution. As a consequence, the different patterns in a scatterer distribution are generated based on the different values of density and shape parameters of the scatterer model. When both α and ρ are smaller, the scatterers are tightly clustered in the tissue space, while the scatterer distributions become stochastic or uniform with the larger values of α and ρ. Thus, it should be simultaneously considered the effects of shape parameter α and density parameter ρ on the scatterer distribution when the scatterer model is established.

To determine the values of the parameters for the scatterer model of CCA with three layers and blood flow, ultrasonic RF signals from scatterer models shown in Fig. 3 are simulated in Field II with the simulation parameters listed in Table I. Then, the statistical histograms and Nakagami distributions based on MLE are computed for the envelope signals. Figure 4 illustrates the histograms, best-fitted curves, and corresponding parameters (mean ± SD) of the Nakagami model over 30 simulations based on the scatterer (Gamma) model with different values of scale parameter α and density parameter ρ, respectively. From this figure, the simulated envelope signals from the scatterer models with different values of scale parameter α and density parameter ρ present different histograms, which are fitted well by the Nakagami distribution with different values of shape parameter m and power parameter u.

On the other hand, the Sonix TOUCH Research ultrasound system (sonixTOUCH; Ultrasonix Medical Corporation, Burnaby, British Columbia, Canada) with a L14-5W/60 linear array transducer is used to scan CCAs of 30 healthy subjects (15 females; age 24–48 yr and 15 males; age 25–54 yr). Before ultrasound examinations, subjects repose quietly for at least 10 min. The detection is best accomplished for the subject with supine position and neck holstered by soft pillows. Table II lists the imaging parameters used in Sonix TOUCH Research. Figure 5 demonstrates a clinical B-mode ultrasound image (right panel) from a CCA with several scan lines of RF (middle panel) and envelope (left panel) signals. In this figure, the box on the image indicates the analyzed region, from which the blood, intima, media, adventitia, and surrounding tissue are segmented, and corresponding envelope signals are extracted. Subsequently, the statistic histograms and the best-fitted curves based on Nakagami model by the MLE algorithm are calculated for the segmented envelope signals.

In Fig. 6, the envelope signals from all four kinds of tissue present different histogram distributions, which are fitted well

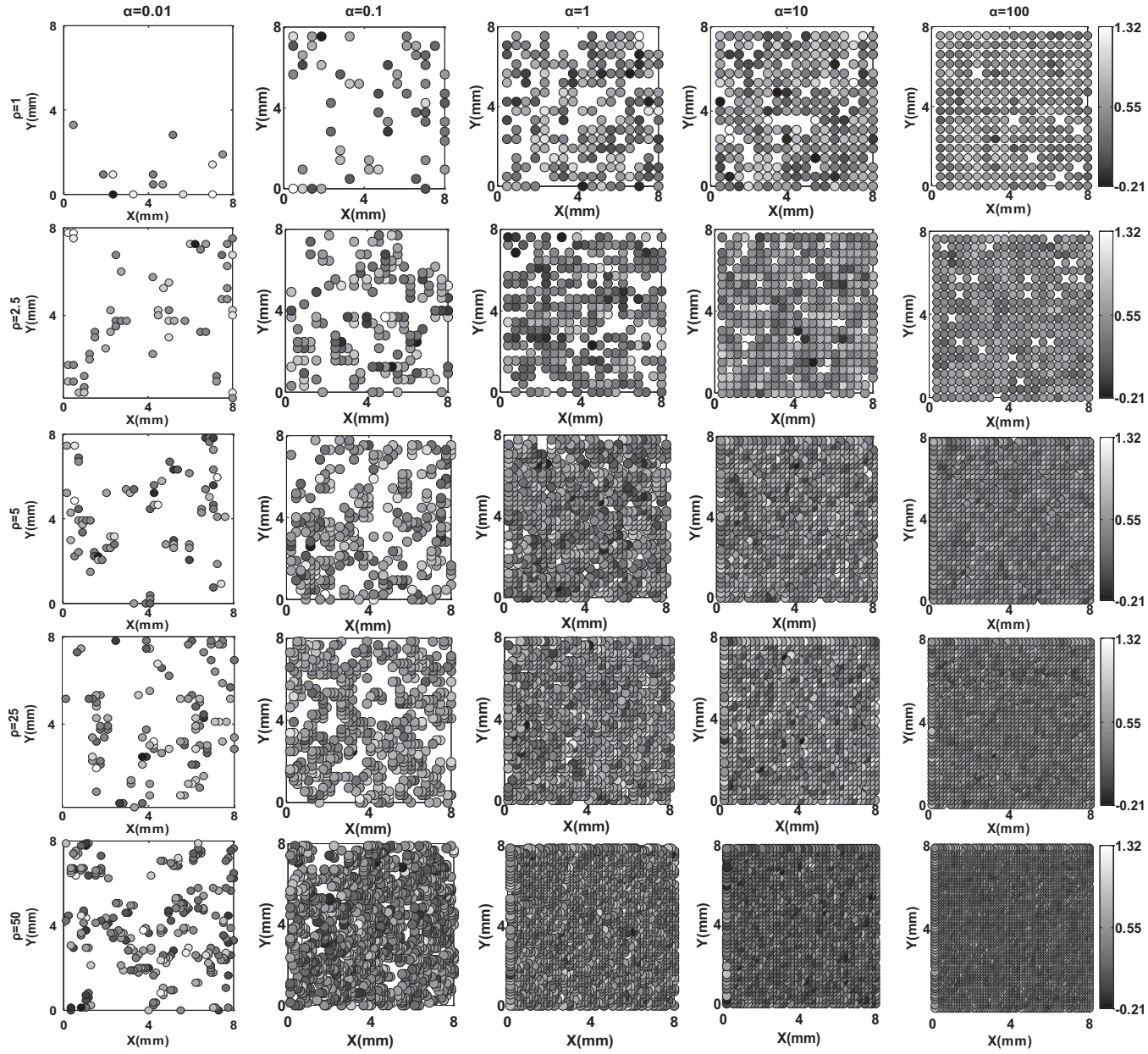

FIG. 3. The scatterer distributions in a size of 8 × 8 mm from the Gamma model with different values of shape parameter α and density parameter ρ.

TABLE I. The ultrasonic simulation parameters used in Field II.

Parameters		Values
Acoustic parameters	Center frequency	10 MHz
	Sampling frequency	100 MHz
	Speed of sound	1,540 m/s
	Wavelength	1.54×10^{-4} m
The parameters for the linear array transducer	Physical elements	512
	Active elements	64
	Element width	1.54×10^{-4} m
	Element height	0.005 m
	Fixed focal point	[0, 0, 0.03] m
	Lines for envelope imaging	50

by the Nakagami distribution with different values of shape parameter m and power parameter u. For the blood signals, the Nakagami parameters $m = 1.36$ and $u = 0.19$ reflect the random speckle distribution from hypoechoic in the analyzed region on the image. The Nakagami parameters for envelope signal of the intima are $m = 1.79$ and $u = 0.26$, which show the more regular speckle distribution and larger average power from the fine and smooth intima with good continuity than those from the blood. To the media envelope signal, the Nakagami parameters, $m = 0.32$ and $u = 0.17$, indicate the more clustered speckle distribution and smaller average power from the hypoechoic tissue band between the intima and adventitia than those of the blood and intima. The Nakagami parameters, $m = 3.88$ and $u = 0.45$, for adventitia reflect the most regular speckle distribution and largest

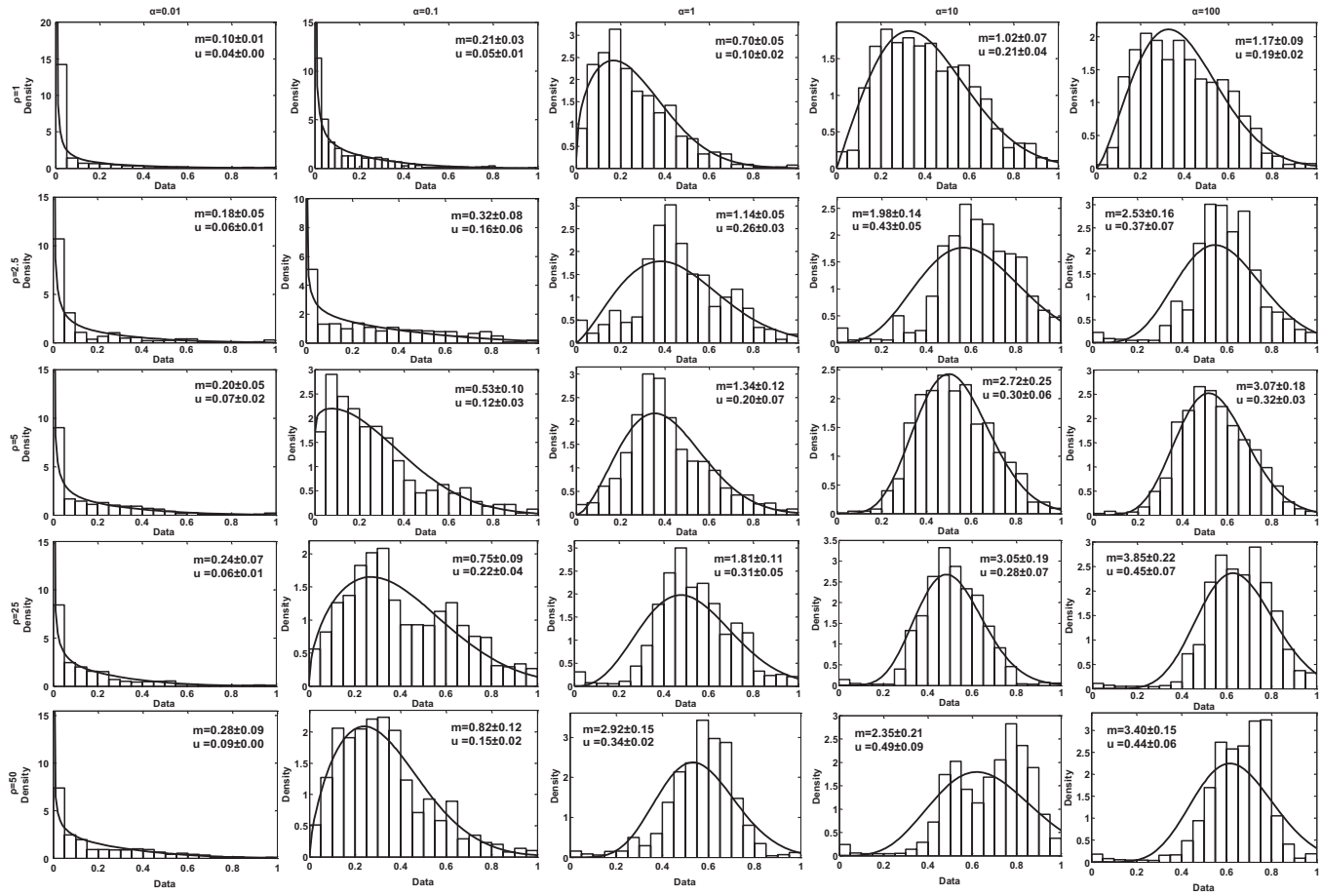

FIG. 4. The histograms, best-fitted curves, and corresponding parameters (mean ± SD) of the Nakagami model over 30 simulations based on the scatterer (Gamma) model with different values of scale parameter α and density parameter ρ, respectively.

TABLE II. The ultrasonic scanning parameters used in Sonix TOUCH research.

Imaging parameters	Values
Center frequency	10 MHz
Sampling frequency	40 MHz
Speed of sound	1,540 m/s
Wavelength	1.54×10^{-4} m
Frame frequency	88 Hz
Dynamic range	70 dB
Sector	100%
Gain	54%
Line density	392

average power from the hyperechoic area in the vessel wall. Table III lists the mean and SD of parameters of fitted curves based on the Nakagami model and mean intensity for the envelope signals of blood, intima, media, and adventitia from 30 clinical results. Compared the parameters in Table III with those of simulated results in Fig. 4, the values of shape parameter α, density parameter ρ, and intensity of the Gamma model for scatterer distribution of each kind of tissue are found and listed in Table IV.

3.B. Imaging simulation for the statics model

According to the related parameters listed in Table IV, 30 cases of the scatterer distributions for the CCA with three layers are built. As an example, Fig. 7(a) shows the scatterer distribution in axial plane from one case, where the surrounding tissue is constituted by the scatterers with the position of a uniform distribution and amplitude of a Gaussian distribution. In this figure, the vessel wall with three layers and blood are clearly constructed. The scatterers for the intima have a higher density but clustered distribution. Oppositely, the adventitial scatterers present a dense and even distribution. However, the intensity of the adventitial scatterer is higher than that of the intimal scatterer. The medial scatterers have the lowest density and intensity as well as the sparsest distribution.

Based on the constructed scatterer model for CCA, Field II with the ultrasound simulation parameters listed in Table II is used to simulate corresponding RF signals, from which envelope signals by Hilbert transform and B-mode images by interpolation and logarithmic compression are yielded. Figure 7(b) shows the B-mode image corresponding to the scatterer model in Fig. 7(a). Figure 7(c) shows a clinical B-mode ultrasound image with scanning parameters listed in Table II

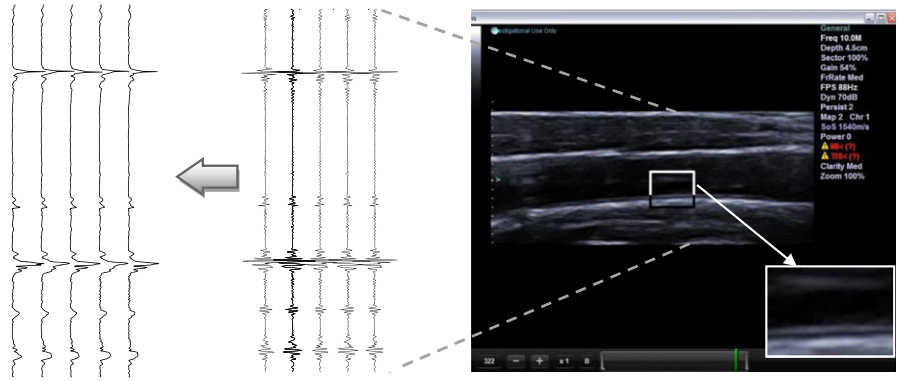

FIG. 5. A clinical B-mode ultrasound image (right panel) from a CCA with several scan lines of RF (middle panel) and envelope (left panel) signals. The box on the image indicates the analyzed region, which is amplified in the lower right corner. [Color figure can be viewed at wileyonlinelibrary.com]

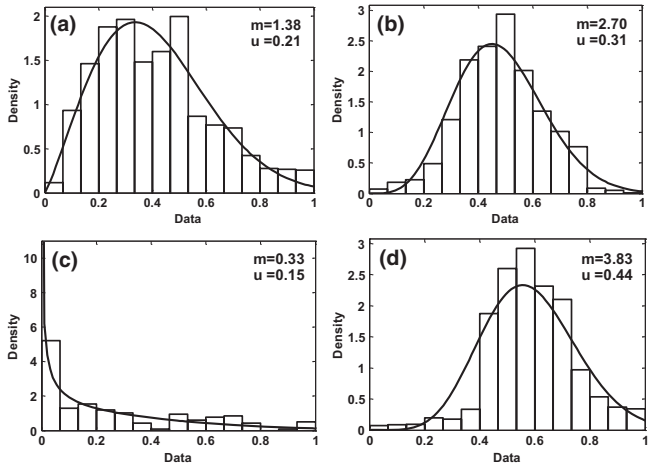

FIG. 6. The histograms, best-fitted curves, and corresponding parameters (mean ± SD) of Nakagami model for the blood (a), intima (b), media (c), and adventitia (d) sampled from the analyzed region of B-mode image in Fig. 5.

for comparison. In the simulation result, three layers, blood, and surrounding tissue of a carotid artery can be distinguished. Speckles similar to those in clinical B-mode ultrasound images can also be found. For the thicknesses of layers, the intima is the thinnest, and the media is the thickest. This result is consistent with that in geometric model of the CCA shown in Fig. 1. To the gray levels, the adventitia is the highest, and the media is the lowest. The intima is lower than the adventitia but higher than the blood. However, both intima and blood belong to hypoechoic tissue. In general, the characteristics of echo intensity for the carotid artery in the simulated B-mode image accord with those of the scatterer model and the observation in clinical B-mode images. With a finely manual segmentation, the geometrical sizes measured from the simulated B-mode images are compared with the preset ones. The maximum relative errors for the diameter of the lumen and the thicknesses of the intima, media, and adventitia are 0.13%, 3.89%, 1.35%, and 0.06%, respectively.

Table V lists the parameters (mean ± SD) of the fitted curves based on the Nakagami model and intensity to the envelope signals of blood, intima, media, and adventitia from 30 simulations for a quantitative evaluation. Compared with the parameters of the clinical examinations listed in Table III, the maximum relative errors for the shape parameter m, average power u, and intensity are 6.52%, 5.13%, and 4.96%, respectively. This means a good agreement between the simulated and clinical results for the speckle distribution and intensity in B-mode images.

TABLE III. The mean and SD of parameters for fitted curves based on the Nakagami model, and mean intensity for the envelope signals of blood, intima, media, and adventitia from 30 clinical results.

Parameter	Lumen	Intima	Media	Adventitia
m (mean ± SD)	1.38 ± 0.12	2.70 ± 0.20	0.33 ± 0.06	3.84 ± 0.10
u (mean ± SD)	0.21 ± 0.04	0.31 ± 0.02	0.15 ± 0.03	0.44 ± 0.06
Intensity ($\times 10^{-2}$)	0.04 ± 0.01	3.24 ± 0.04	0.04 ± 0.00	6.25 ± 0.01

TABLE IV. The shape parameter α and density parameter ρ of the Gamma model as well as mean intensity for the scatterer distribution of the CCA with three layers.

Parameter	Lumen	Intima	Media	Adventitia
α	1	10	0.1	100
ρ	5	5	2.5	25
Intensity ($\times 10^{-2}$)	0.04	3.24	0.04	6.25

3.C. Imaging simulation for the pulsatile model

The elastic carotid wall suffers radial deformation in the form of expansion and contraction with a pulsation of blood pressure during a cardiac cycle *in vivo*. To get the displacement of the radial movement for vascular wall, the mean blood pressure $P_{mean}(t) = 1.03 \times 10^4$ Pa and a measured blood pressure waveform during a cardiac cycle $P(t)$ shown in Fig. 8(a)[32] are substituted into Eq. (4). The internal and

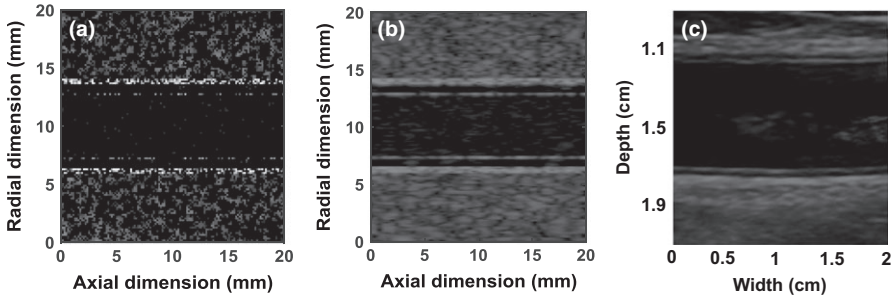

FIG. 7. A scatterer distribution (a), the corresponding B-mode ultrasound image (b), and a clinical B-mode ultrasound image (c) with the center frequency of 10 MHz for the CCA with three layers, respectively.

TABLE V. The parameters (mean ± SD) of the fitted curves based on the Nakagami model, and mean intensity to the envelope signals of blood, intima, media, and adventitia from 30 simulations.

Parameter	Lumen	Intima	Media	Adventitia
m (mean ± SD)	1.37 ± 0.10	2.72 ± 0.16	0.34 ± 0.03	3.85 ± 0.08
u (mean ± SD)	0.20 ± 0.02	0.30 ± 0.05	0.16 ± 0.04	0.44 ± 0.03
Intensity ($\times 10^{-2}$)	0.04 ± 0.01	3.24 ± 0.04	0.04 ± 0.00	6.25 ± 0.01

external radii of the vascular wall are $R_i = 2.625$ mm and $R_o = 3.675$ mm, respectively. The elastic modules of IM and adventitia are 500,000 Pa and 100,000 Pa,[28] respectively. According to the Hooke's law, the elastic module for the total vascular wall could be set as $E = 60{,}0000$ Pa, which is a sum of the elastic modules of the IM and adventitia. With these parameters, the radial displacements for the arterial wall (including all three layers) waveforms of lumen (dashed line) during a cardiac cycle of 1 s are computed by Eq. (4). Meanwhile, the IM is compressed with an increase in blood pressure and then recovered during diastole.[10] The curve of the IM thickness during a cardiac cycle measured from human subjects is shown in Fig. 8(b)[10] to describe this variation. An extra movement calculated according to the variation in the IM thickness is added to the obtained displacements of intima and media, respectively. The maximum compression is 0.06 mm corresponding to the peak of pressure at 0.32 s in the cardiac cycle of 1 s. The distention waveforms of lumen (dashed line) and adventitia (solid line) during a cardiac cycle of 1 s are shown in Fig. 8(c). It can be found that the lumen deformation is larger for the same blood pressure due to considering the extra movement caused by the IM compression. A waveform of axial displacement of IM varying with blood pressure during a cardiac cycle shown in Fig. 9 is directly used as the theoretical displacement curve for the simulation. This waveform is obtained from healthy subjects using the clinical carotid ultrasound.[10]

With the predetermined velocity of axial centerline v_0, the distribution of the blood flow is calculated using the Eq. (5). As the blood flow is influenced by the pulsatile pressure, a velocity waveform of axial centerline from CCAs of healthy subjects[33] shown in Fig. 10(a) is obtained using clinical carotid ultrasound to describe the pulsatile blood flow. The profile of velocity computed by Eq. (5) with $v_0 = 0.5$ m/s at 0.2 s is shown in Fig. 10(b). The parabolic profile means that the velocity is zero at the vascular wall and increases to maximum at the axial centerline position of lumen.

The curves for radial displacements of IM and adventitia, axial displacement of IM, and velocity profile of blood flow during a cardiac cycle are applied to the established scatterer model for CCA with the intima, media, adventitia, and blood. The scatterers at a different position correspondingly move in chronological order. Fifty pulsatile scatterer models of the CCA with three layers and blood flow are constructed with the frame frequency of 50 Hz. Subsequently, 50 B-mode sequence images are simulated using Field II with the simulation parameters listed in Table II. By extracting the envelope signal of the 25th line from each frame, 30 M-mode ultrasound images for the dynamical CCA models during a cardiac cycle of 1 s are obtained. As an example, one of them is

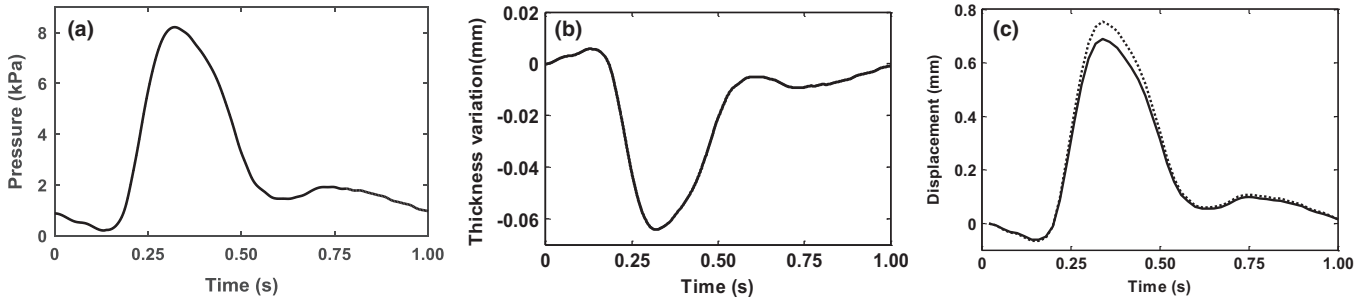

FIG. 8. The theoretical curves of pressure (a), the thickness variation in IM (b), the distention of lumen (dashed line) and adventitia (solid line) (c) for the simulation of dynamical CCA during a cardiac cycle of 1 s.

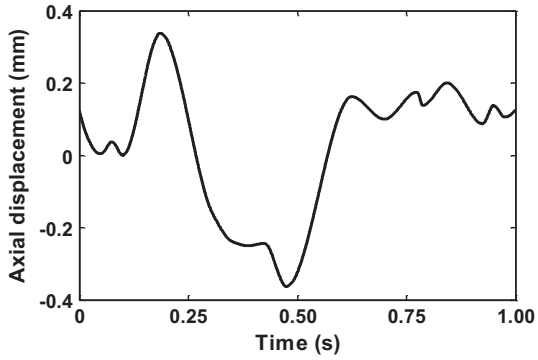

FIG. 9. The theoretical curve of axial displacement of IM for the simulation of dynamical CCA during a cardiac cycle of 1 s.

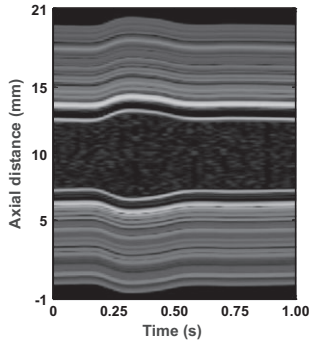

FIG. 11. The simulated M-mode ultrasound image from the dynamical CCA model during a cardiac cycle of 1 s.

shown in Fig. 11. The fluctuations for intima, media, and adventitia of the carotid artery during a cardiac cycle could be clearly distinguished in the simulated M-mode image. Moreover, the IM and adventitia present a difference of distensible displacements, which is caused by a reduced thickness of IM during the systole period and a recovery in the diastole period. This is consistent with the preset model shown in Fig. 8.

Thirty sets of sequences of B-mode images with frame frequency of 50 Hz are randomly generated. The envelope signals are segmented based on a grayscale threshold method[34] to yield the intimal, medial, and adventitial boundaries for each image. Then, the curves of radial displacements of the lumen and adventitia as well as the IM thickness during a cardiac cycle are calculated. Figure 12 shows the estimated curves with error bars (solid line) plotted with theoretical curves (dashed line) for the distention of lumen (a), adventitia (b), and the IM thickness (c) based on 30 simulations. In general, three curves estimated from the simulated images are in agreement with the theoretical ones. The NRMSEs for the distension of lumen and adventitia and the IM thickness between the estimated and theoretical versions are 0.09 ± 0.02, 0.02 ± 0.00, and 0.68 ± 0.08, respectively. It should be noted that the measured IM thickness has a larger deviation because the accuracy is poor during the upstroke of the systole period and downstroke of the diastole period. This means that the detection of a variation in the IM thickness during a cardiac cycle is still a big challenge.

To evaluate the movement of IM in the axial direction for the simulated results, the block tracking algorithm[35] is used to extract the axial motion of intima-media. According to this algorithm, a kernel with size of 0.10×0.10 mm in the first frame is selected to cover a region of IM. Then, a window with 0.70×0.70 mm is defined as the search area in the succeeding frames. The position of the search windows is corrected by the theoretical radial displacement of IM shown in Fig. 9 to protect the detection from the radial motion of the vessel wall. Figure 13 gives the estimated curves with error bars (solid line) plotted with the theoretical ones (dashed line) for the axial displacement of IM based on 30 simulations. This axial movement of IM for the simulated results is generally consistent with the theoretical one. The NRMSE between the estimated and theoretical results is 0.05 ± 0.01.

The velocity of blood flow is evaluated using its profile approximation, which is obtained with a standard velocity estimation technique, the autocorrelation technique,[36] from the simulated data. A fifth-order Butterworth high-pass filter (HPF) with a cutoff frequency of 150 Hz is applied to the demodulated signals to yield Doppler blood flow signals. The Doppler lines are calculated from ten consecutive RF

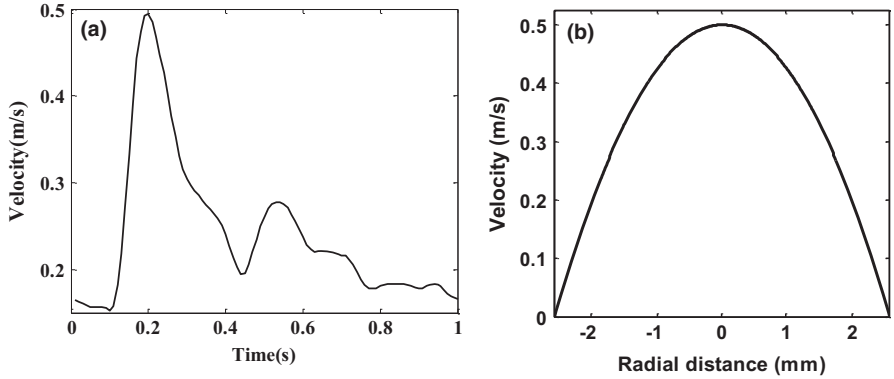

FIG. 10. The velocity waveform of axial centerline (a) and the parabolic velocity profile with $v_0 = 0.5$ m/s at 0.2 s (b) for the simulation of blood flow during a cardiac cycle of 1 s.

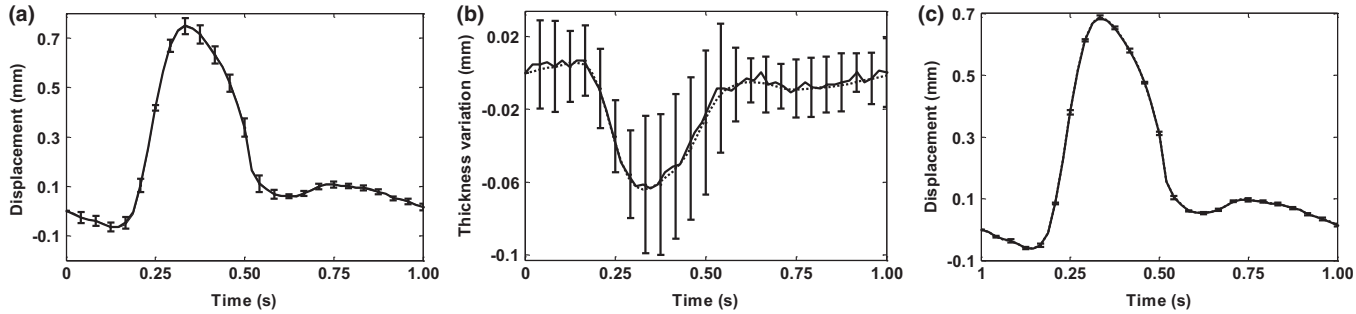

FIG. 12. The estimated curves with error bars (solid line) plotted with the theoretical ones (dashed line) for the distention of IM (a), the thickness variation in IM (b), and the distention of adventitia (c) based on 30 simulations.

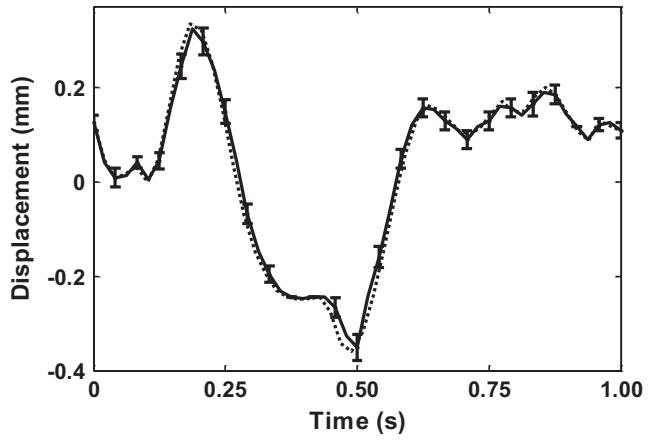

FIG. 13. The estimated curve with error bars (solid line) plotted with the theoretical one (dashed line) for the axial displacement of IM based on 30 simulations.

echo lines at a pulse repetition frequency of 10 kHz. Figure 14 shows the estimated profile with error bars (solid line) plotted with the theoretical one (dashed line) for the maximum velocity at axial centerline of 0.5 m/s based on 30 simulations. As the blood flow signals with lower frequencies are removed by HPF, the estimated blood flow velocities close to the vessel walls are poorer accurate. A larger NRMSE of 0.17 ± 0.04 between the estimated and theoretical results is yielded.

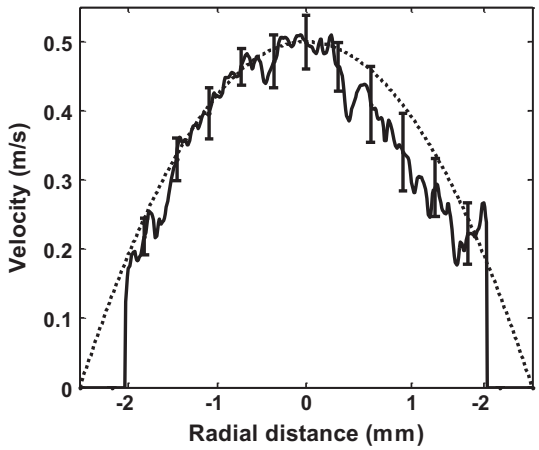

FIG. 14. The estimated velocity profile with error bars (solid line) plotted with the theoretical one (dashed line) for the maximum velocity at axial centerline of 0.5 m/s based on 30 simulations.

This article presents an ultrasound simulation model for the CCA with three layers for validation of 2D wall motion and blood velocity estimation algorithms. The model describes not only characteristics of echo distributions conforming to clinical ones but also a varying thickness of IM, and displacements in both axial and radial directions with pulsatile blood pressure during a cardiac cycle. Thus, this model is capable of reflecting the textural, acoustic, and dynamic characteristics of blood vessels and could be useful for verifying the validities and superiorities of detection algorithms. However, it still remains some limitations including: (a) Rigid generalized cylinders are used to model the lumen, three layers, and surrounding tissue of CCA, and thus, the local irregularity and deformation of vessel walls are not considered. (b) Only the distance between the intima and adventitia layer (media thickness) varies with the blood pressure during a cardiac cycle. This means that presented model could not use to evaluate the strain estimation for vessel walls. (c) Only the simulation from the longitudinal view is performed. In clinic applications, CCAs can also be scanned from the transverse view for diagnosis. In this case, the scatterer distribution and amplitude characteristics for transverse plane simulation are varied over the vessel circumference. Thus, the present simulation is unrealistic to reflect the CCA features from the transverse view. (d) The computation load of the simulation is high. Under Windows 2007 (Microsoft corporation; Redmond, WA, USA) and Matlab 7. 14 (The MathWorks, Inc.; Natick, MA, USA) running on a PC with i5 processor and a 3.2 GHz processor with 4 GB RAM, the time for simulating RF signals and B-mode image sequences of 50 frames are approximate 38 h. These limitations would be the next research orientations in future.

4. CONCLUSION

This paper presents an ultrasound simulation model for the CCA with three layers for validation of 2D wall motion

and blood velocity estimation algorithms. This model describes not only characteristics of echo distributions conforming to clinical ones but also a varying thickness of IM, and displacements in both axial and radial directions with pulsatile blood pressure during a cardiac cycle. Based on a geometrical structure and clinical data of CCAs, a 3D scatterer phantom is constructed. The dynamic scatterer model is realized by moving the scatterers in chronological order according to the theoretical curves in both axial and radial directions. Finally, Field II is used to simulate RF echo data and then yield B-mode ultrasound images. The quantitative evaluations based on the static and dynamic simulated images indicate that the simulation results present the static sizes and dynamical variations for the IM, adventitia, and blood flow of the CCA in accordance with the preset values; the echo distributions also conform to clinical versions. Therefore, the presented simulation model could be useful as a data source to evaluate the performance of studies on measurement algorithms of ultrasound-based tissue structures and dynamic parameters for the CCA layers.

ACKNOWLEDGMENTS

This work was supported by National Natural Science Foundation of China under Grants Nos. 81771928 and 61561049.

[a]Author to whom correspondence should be addressed. Electronic mail: yfengzhang@yahoo.com.

REFERENCES

1. Blacher J, Guerin AP, Pannier B, Marchais SJ, Safar ME, London GM. Impact of aortic stiffness on survival in end-stage renal disease. *Circulation*. 1999;99:2434–2439.
2. Bots ML, Hoes AW, Hofman A, Witteman JCM, Grobbee DE. Cross-sectionally assessed carotid intima–media thickness relates to long-term risk of stroke, coronary heart disease and death as estimated by available risk functions. *J Intern Med*. 1999;245:269–276.
3. Meer IMVD, Bots ML, Hofman A, Sol AID, Kuip DAMVD, Witteman JCM. Predictive value of noninvasive measures of atherosclerosis for incident myocardial infarction: the Rotterdam study. *Circulation*. 2004;109:1089–1094.
4. Lusis AJ. Atherosclerosis. *Nature*. 2000;407:233–241.
5. Rodriguez-Macias KA, Lind L, Naessen T. Thicker carotid intima layer and thinner media layer in subjects with cardiovascular diseases: an investigation using noninvasive high-frequency ultrasound. *Atherosclerosis*. 2007;189:393–400.
6. Falk E, Thim T, Kristensen IB. Atherosclerotic plaque, adventitia, perivascular fat, and carotid imaging. *JACC Cardiovas Imaging*. 2009; 2:183–186.
7. Persson M, Ahlgren AR, Jansson T, Eriksson A, Persson HW, Lindström K. A new non-invasive ultrasonic method for simultaneous measurements of longitudinal and radial arterial wall movements: first in vivo trial. *Clin Physiol Funct Imaging*. 2003;23:247–251.
8. Cinthio M, Ahlgren AR, Jansson T, Eriksson A, Persson HW, Lindström K. Evaluation of an ultrasonic echo-tracking method for measurements of arterial wall movements in two dimensions. *IEEE Trans Ultrason Ferroelectr Freq Control*. 2005;52:1300–1311.
9. Cinthio M, Ahlgren AR. Intra-observer variability of longitudinal displacement and intramural shear strain measurements of the arterial wall using ultrasound noninvasively in vivo. *Ultrasound Med Biol*. 2010;36:697–704.
10. Ahlgren AR, Cinthio M, Persson HW, Lindström K. Different patterns of longitudinal displacement of the common carotid artery wall in healthy humans are stable over a four-month period. *Ultrasound Med Biol*. 2012;38:916–925.
11. Ilea DE, Duffy C, Kavanagh L, Stanton A, Whelan PF. Fully automated segmentation and tracking of the intima media thickness in ultrasound video sequences of the common carotid artery. *IEEE Trans Ultrason Ferroelectr Freq Control*. 2013;60:158–177.
12. Lee KW, Wood NB, Xu XY. Ultrasound image-based computer model of a common carotid artery with a plaque. *Med Eng Phys*. 2004;26:823–840.
13. Balocco S, Basset O, Azencot J, Tortoli P, Cachard C. 3D dynamic model of healthy and pathologic arteries for ultrasound technique evaluation. *Med Phys*. 2008;35:5440–5450.
14. Warriner RK, Johnston KW, Cobbold RSC. A viscoelastic model of arterial wall motion in pulsatile flow: implications for Doppler ultrasound clutter assessment. *Physiol Meas*. 2008;29:157–179.
15. Larsson M, Kremer F, Claus P, Kuznetsova T, Brodin LA, Dhooge J. Ultrasound-based radial and longitudinal strain estimation of the carotid artery: a feasibility study. *IEEE Trans Ultrason Ferroelectr Freq Control*. 2011;58:2244–2251.
16. Solomou R, Loizou CP, Kasparis T. Ultrasound common carotid artery video simulation and motion analysis. In: Kyriacou E., Christofides S., Pattichis C. (Eds), *XIV Mediterranean Conference on Medical and Biological Engineering and Computing 2016*: IFMBE Proceedings, Paphos, Cyprus, March 31st-April 2nd 2016 (Vol. 57, pp. 347–350). Berlin, Germany: Springer.
17. Fekkes S, Swillens AES, Hansen HHG, et al. 2-D versus 3-D cross-correlation-based radial and circumferential strain estimation using multiplane 2-D ultrafast ultrasound in a 3-D atherosclerotic carotid artery model. *IEEE Trans Ultrason Ferroelectr Freq Control*. 2016;63:1543–1553.
18. Stoitsis J, Golemati S, Koropouli V, Nikita KS. Simulating dynamic B-mode ultrasound image data of the common carotid artery. Imaging Systems and Techniques, Ist, IEEE International Workshop on IEEE, Chania, Greece, 10-11 September 2008: 144-148.
19. Jensen JA. FIELD: a program for simulating ultrasound systems. *Med Biol Eng Comput*. 1996;34:351–353.
20. Fung Y-C. *Biomechanics: Mechanical Properties of Living Tissues* (2nd edn). Springer, Berlin: Springer Science+Business Media; 2005.
21. Neyman J, Scott EL. A theory of the spatial distribution of galaxies. *Astrophys J*. 1952;116:144–163.
22. Lafferty JD. Gibbs-Markov Models. *Computing Science & Statistics Proceedings of Symposium on the Interface Foundation*; 1995, 370–377.
23. Cramblitt RM, Parker KJ. Generation of non-Rayleigh speckle distributions using marked regularity models. *IEEE Trans Ultrason Ferroelectr Freq Control*. 1999;46:867–874.
24. Miller FP, Vandome AF, Mcbrewster J. *Hilbert Curve*. Saarbrücken, Germany: Alphascript Publishing; 2010.
25. Thijssen JM. Ultrasonic speckle formation, analysis and processing applied to tissue characterization. *Pattern Recogn Lett*. 2003;24:659–675.
26. Nakagami M. Statistical character of short-wave fading. *J Inst Elec Commun Engrs*. 1943;27:145–150.
27. Redner RA, Walker HF. Mixture densities, maximum likelihood and the EM algorithm. *SIAM Rev*. 1984;26:195–239.
28. Cinthio M, Ahlgren AR, Bergkvist J, Jansson T, Persson HW, Lindstrom K. Longitudinal movements and resulting shear strain of the arterial wall. *Am J Physiol Heart Circ Physiol*. 2006;291:H394–402.
29. McDonald DA. *Blood Flow in Arteries* (2nd edn). London, England: Edward Arnold; 1974.
30. Patel DJ, Fry DL. The elastic symmetry of arterial segments in dogs. *Circ Res*. 1969;24:1–8.
31. Fung YC. *Biomechanics: Circulation* (2nd edn). New York, NY: Springer; 1997.
32. Zhang Y, Gao Y, Wang L, Chen J, Shi X. The removal of wall components in Doppler ultrasound signals by using the empirical mode decomposition algorithm. *IEEE Trans Biomed Eng*. 2007;54:1631–1642.

33. Gao L, Zhang Y, Zhang K, Cai G, Zhang J, Shi X. A computer simulation model for Doppler ultrasound signals from pulsatile blood flow in stenosed vessels. *Comput Biol Med*. 2012;42:906–914.
34. Chan TF, Shen J. *Image Processing and Analysis*. Beijing, China: Science Press; 2009.
35. Parker KJ, Gao L, Lerner RM, Levinson SF. Techniques for elastic imaging: a review. *IEEE Eng Med Biol Mag*. 1996;15:52–59.
36. Kasai C, Namekawa K, Koyano A, Omoto R. Real-time two-dimensional blood flow imaging using an autocorrelation technique. *IEEE Trans Sonics Ultrason*. 1985;32:458–464.

SUPPORTING INFORMATION

Additional Supporting Information may be found online in the supporting information tab for this article.

Video S1. Simulated B-mode sequence images and corresponding RF signals.